Journal of the Serbian Chemical Society
JSCS-info@shd.org.rs • www.shd.org.rs/JSCS
J. Serb. Chem. Soc. *88* (3) 283–300 (2023)
JSCS–5626
Original scientific paper
Published 14 December 2022

Highly efficient functional materials for modern electrochemical devices

VITALY SMILYK*, YULIIA VOLOSHANOVSKA, VADYM GALAGUZ, OLEKSANDR IVANENKO and OLHA MEDVEZHYNSKA

V. I. Vernadsky Institute of General and Inorganic Chemistry of the National Academy of Sciences of Ukraine, 32-34 Acad. Palladina Ave., Kyiv, 03142, Ukraine

(Received 27 July, revised 15 November, accepted 21 November 2022)

Abstract: In order to find new functional materials and materials with improved performance for next-generation electrochemical devices, several new materials for various purposes have been synthesized. In particular, $BiVO_4$ films were obtained by electrochemical synthesis using interferometric control of film thickness during their deposition. Previously, it was found that the use of thin $BiVO_4$ films with a thickness of 150 to 400 nm is most effective, where an increase in the quantum yield of photocurrent up to 0.25 at λ of 400 to 450 nm was observed. $LiFePO_4$ was synthesized in DES medium (low-temperature eutectic solvents): choline chloride–triethylene glycol (ChCl–TEG) and choline chloride–ethylene glycol (ChCl–EG) using NH_4FePO_4 and CH_3COOLi as precursors. It was found that the mode of synthesis of $LiFePO_4$/C at 973 K for 1 h does not lead to oxidation of $LiFePO_4$, as evidenced by the values of the ratio Fe^{2+}/Fe^{3+} for $LiFePO_4$ and $LiFePO_4$/C, which are 2.4 and 2.7, respectively. It was found that the substitution of a part of lead cations (up to 20 mol. %), in the composition of the fluoride-conducting phase $Pb_{0.86}Sn_{1.14}F_4$, contributes to the increase of its conductivity in the whole temperature range, the higher the concentration of the substituent, to a greater extent. Charge transfer is provided by highly mobile interstitial fluorine anions, the concentration of which increases with the rise of temperature and substituent content.

Keywords: heterostructure; electrodeposition; photoelectrochemical conversion; solid fluoride-ion conductors; quantum yield; photocurrent.

INTRODUCTION

Current trends require quick and high-quality solute to problems of various kinds, and the ever-growing global demand for energy is attracting more and more attention to alternative energy solutions that will remain viable in the long turn. Therefore, one of the actual tasks today is the development and creation of

* Corresponding author. E-mail: VitaliySmilyk@i.ua
https://doi.org/10.2298/JSC220729082S

new and promising materials with improved characteristics for alternative sources of energy storage and conversion, sensors and ion-selective electrodes for detection of compounds in gaseous atmospheres, aqueous solutions or melts, environmental monitoring.[1–12] These include, in particular, solid-state fluoride--ion and lithium-ion current sources, solar energy converters, photoelectrochemical devices for the decomposition of organic compounds.

$BiVO_4$ is a promising and easy-to-obtain materials for converting solar energy into electricity.[13–15] Unlike chalcogenides and some oxides, $BiVO_4$ is a more advantageous material because these compounds contain cadmium and lead. In addition, there is an urgent need to increase the stability of semiconductor sensitizers based on widely used cadmium sulfide and selenide.[16] $BiVO_4$ has recently attracted increasing attention as a photosensitive material due to the fact that it is a straight-band semiconductor with high absorption of light in the visible region of the solar spectrum.

To create efficient lithium-ion current sources, it is advisable to use nanocrystalline iron (II) phosphate as a cathode material, because, it has high thermal stability and environmental safety.[17–19] The cathode based on it has a large resource during cycling and a high theoretical capacity. However, obtaining $LiFePO_4$, with the necessary properties (single-phase, crystalline, nanoscale, with a conductive coating) is quite a difficult task. Thus, large-scale use of $LiFePO_4$ as an electrode material is hampered by the disadvantages of commercial synthesis methods, which include a long high-temperature stage of crystal structure formation, which leads to oxidation of iron (II) and recrystallization of $LiFePO_4$ powder.[20] Therefore, it is important to modify existing and develop new methods for obtaining nanocrystalline $LiFePO_4$ powders with a conductive carbon coating.[21,22]

Given the depletion of natural resources to increase the production of known energy generating systems (lithium power sources), the development and production of alternative new power sources have not only great scientific and technical, but also social and economic significance. The development of advanced fluoride batteries requires the creation of new electrode and electrolyte materials that have not only a high unipolar conductivity of fluoride in the temperature range close to room temperature, but also a wide window of electrochemical potentials, which provides rapid reversible transfer of fluorides across the interface between the phases of the electrode/electrolyte without destroying their structure. The problem of creating flexible and thin-layer electrode and electrolyte fluoride-conducting materials requires a separate solution.

It follows that the development and creation of new functional materials and materials with improved performance for the next-generation electrochemical devices is an urgent problem today, and its solution should not be scientific only, but also practical and feasible.

EXPERIMENTAL

Electrochemical deposition of $BiVO_4$ films was performed in galvanostatic mode with a platinum counter electrode. Before electrodeposition of the films, the SnO_2 substrate on the glass was degreased for 5 min in 2M NaOH solution and washed with distilled water. $BiVO_4$ films were obtained at an anode current of 0.5 mA cm^{-2} from an acidic (HNO_3) electrolyte pH 4.7 based on 10 mmol $Bi(NO_3)_3$ and 35 mmol $VOSO_4$. The obtained $BiVO_4$ films were annealed in the air for three hours at 773 K.[15,23]

The structure of the films was investigated by X-ray phase analysis on a DRON-4 diffractometer. The film thickness was measured by scanning electron microscopy with elemental analysis of the film thickness by oxygen on an EVO 50 XVP microscope. The quantum yield of photoelectrochemical current (η) was measured using an installation that included a monochromator MDR-2 and a xenon lamp DKSSH-500 (Fig. 1). Installation and method for measuring the value of η is described in literature.[24] The measurements of electrochemical and photoelectrochemical properties of the films were performed using a potentiostat PGSTAT Elins and the installation shown in Fig. 1. Platinum was used as a counter electrode, films as a working electrode, and Ag/AgCl as a reference electrode; studies of the properties of the films were performed in 0.1 M Na_2SO_4 solution. The stoichiometry of the films was determined using energy-dispersive X-ray spectroscopy based on a scanning electron microscope Philips cpxl 30.

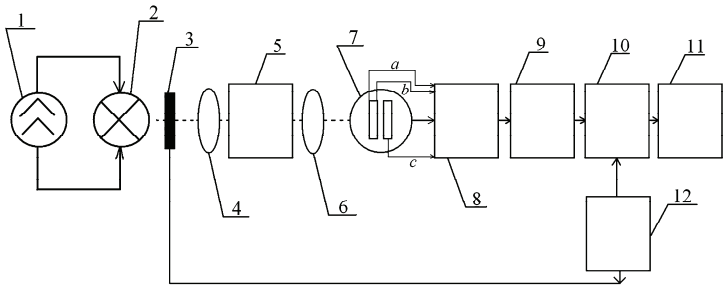

Fig. 1. Scheme for measuring the spectrum of photoelectrochemical current: 1 – power source of the lamp; 2 – xenon lamp of a high pressure of DKSSh–500; 3 – light modulator; 4 – quartz lens; 5 – monochromator MDR–2; 6 – quartz lens; 7 – electrochemical quartz cell (where a – photoelectrode; b – reference electrode; c – counterelectrode); 8 – potentiostat PI–50–1; 9 – amplifier of alternating current U2-8; 10 – phase–sensitive detector UPI-1; 11 – recorder; 12 – alternating current generator.

From X-ray phase analysis of film powder samples (Fig. 2) it was found that after annealing at 773 K in $BiVO_4$ a monoclinic structure is formed, which is sensitive to visible light at wavelengths of 450–600 nm.[25]

In order to measure the optical absorption spectra, namely transmission and reflection, it is advisable to use the $BiVO_4/SnO_2$ heterostructure, since it is a transparent substrate for which the spectral dependences on the transmission can be measured. This heterostructure is a promising model for use in smart glass. Despite the fact that the adhesion to the substrate in this case is slightly worse than in the same heterostructure based on $BiVO_4/TiO_2$, but the use of $BiVO_4/SnO_2$ is much higher than in $BiVO_4/TiO_2$.

According to the results of energy dispersion analysis (Fig. 3) of the spectrum of bismuth vanadate, it was found that the content of stannous dioxide is dominant with the inclusion of bismuth in vanadium.

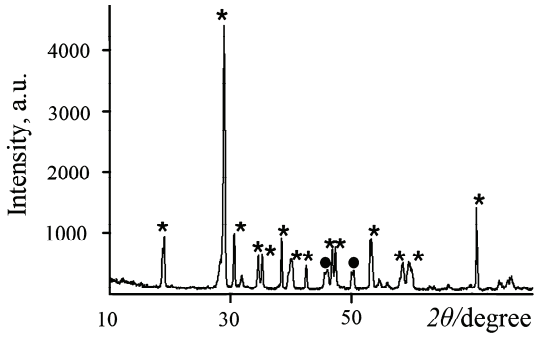

Fig. 2. Diffraction pattern of powder from $BiVO_4$ films treated at a temperature of 500 °C: * - structure of monoclinic $BiVO_4$, ● – tetragonal $BiVO_4$.

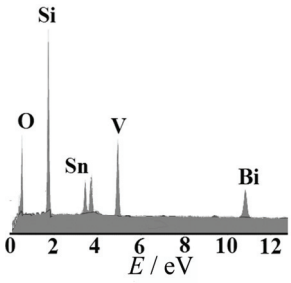

Fig. 3. EDAX spectrum of $BiVO_4/SnO_2$ electrode elements.

Polycrystalline samples based on lead and stanum fluorides were synthesized by the fusion method. Pre-dried and ground samples of starting fluorides were fused in a platinum crucible in an argon atmosphere in the range of 773–823 K and kept at this temperature for 15 min and cooled in the oven off mode (cooling rate 3–5 °C/min).

The electrical conductivity properties of the synthesized samples of fluoride-conducting phases were investigated by the electrochemical impedance spectroscopy using a two-electrode circuit using an autochemical module Autolab (Ekochemie) and a frequency response analyzer (FRA) in the frequency range of 10^{-1}–10^6 Hz at the signal frequency. The pressed polycrystalline cylindrical samples with a diameter of 8 mm and a thickness of 2.0–3.0 mm were used for research. Platinum plates were used as current leads to the samples. The measurements were performed in an argon atmosphere in the range of 298–773 K after thermostating in the cooling mode. To level the contribution of the porosity of the samples, the tablets were made in the same molds from fine fractions with a particle size of not more than 60 μm at a pressure of 150 at. The specific conductivity was calculated as:

$$\sigma = (l/s)R \quad (1)$$

where l is the thickness of the cylindrical sample, s is the contact area, R is the active resistance.

Lithium iron phosphate $LiFePO_4$ was obtained by thermal heating in choline chloride and DEG, which was performed on a magnetic stirrer with a thermostat and the ability to heat up to 623 K. A mixture of choline chloride with ethylene glycol or choline chloride with triethylene glycol (1:2) was placed in a heat-resistant Simax conical flask under reflux/with reflux condenser and kept for 1 h at 353 K and 300 rpm. Then ammonium iron (II) phosphate and lithium precursor were added and heated to 473–573 K and kept for 1–4 h. After synthesis, the precipitate was washed in distilled water and isopropyl alcohol. The obtained powder was dried for 2 h at 393 K.

The method of galvanostatic cycling (cyclic charge–discharge) was used to obtain information about the amount of electric charge stored or given per unit mass of material, and the stability of this parameter during cycling. The current was determined according to the mass of the cathode and set with a resolution of 0.1 μA, the accuracy of maintaining a given current was 0.5 μA. The potential limits were set according to the requirement of the experiment and the capabilities of the electrolyte. The specific capacity was calculated as the product of the set current for the operating time divided by the mass of pure cathode material $LiFePO_4$ in the working electrode. The maximum relative error of determination was 4 %.

RESULTS AND DISCUSSION

Surface studies and spectral dependences of $BiVO_4$

To increase the efficiency of bismuth vanadate, it is necessary to know such parameters as current density and crystallite size. From the study of $BiVO_4$ thin films by scanning electron microscopy (Fig. 4) it was found that the obtained films consist of plate crystals with a plate thickness of about 20 nm. From the photomicrographs (Fig. 4b) it was determined that the size of the crystals depends on the current density of the electrodeposition $BiVO_4$. Fig. 4 shows that an increase in the electrodeposition current leads to an increase in the size of the plate crystals from 60–100 nm to 300–500 nm and a decrease in the developed surface of the film. Analysis of the obtained data leads to the conclusion that the control of such parameters of electrodeposition of $BiVO_4$ films as current density and, to some extent, the concentration of electrolyte components, promotes the formation of nanoscale crystallites and increase the surface area. As will be shown below (Fig. 5), the quantum yield of the photocurrent directly depends on the film thickness.

The band gap/forbidden zone of a semiconductor material such as $BiVO_4$ with direct transitions can be estimated using the Taus equation, where the extrapolation to *x*-axis of the linear region of the graph $(ahv)^2$ related to the electron

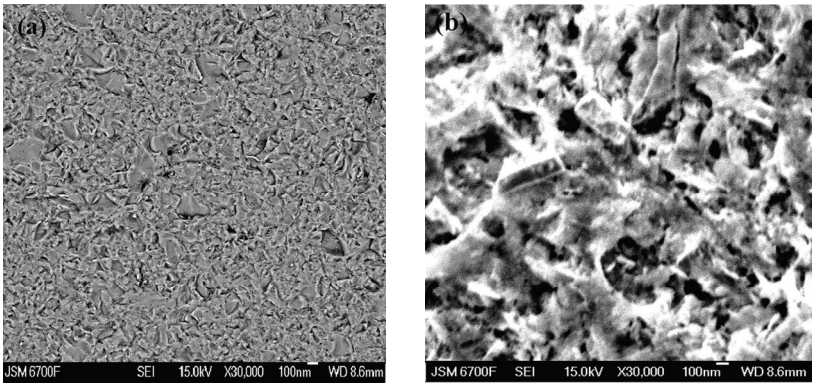

Fig. 4. SEM of the samples of films with a thickness of 140 nm (a) and 1 μm (b), obtained by electrodeposition for 30 min at a current density of 0.5 (a) and 3 mA cm^{-2} (b) with subsequent annealing at 773 K.

energy in eV gives a direct band gap.[26] The optical band gap (E_g), which was previously estimated, is 2.5–2.3 eV, which corresponds to a value of 2.4 eV, which is given in the literature for the monoclinic scheelite $BiVO_4$.[26–28]

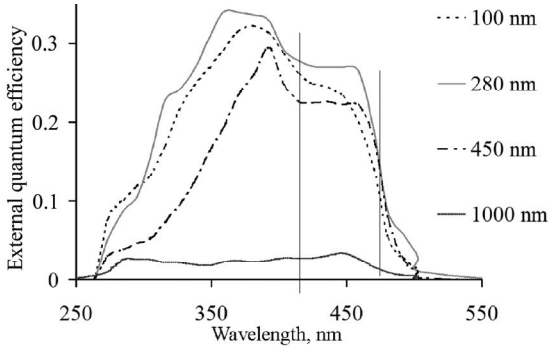

Fig. 5. Spectra of quantum yield of photocurrent of $SnO_2/BiVO_4$ films of different thickness in a solution of 0.1 M Na_2SO_4 at a potential of 0.8 V *vs*. Ag/AgCl.

The studies of the effect of $BiVO_4$ film thickness on the quantum yield of photocurrent (Fig. 5) showed that 0.5–1 μm thick films have a lower quantum yield compared to 80–150 nm thick films. This fact can be explained by the physical properties of polycrystalline $BiVO_4$ films, namely their low conductivity.[29,30] In addition as can be seen from the spectra of Fig. 5, on thin films, a greater contribution to the photocurrent gives visible light compared to films thicker than 500 nm, where the area of maximum quantum yield of the photocurrent falls on the near-ultraviolet radiation.

In $BiVO_4$ films[31] high efficiency is observed at small thicknesses of ~100 nm (Fig. 5). The increase in thickness leads to an increase in energy costs for recombination losses and an increase in their electrical resistance and, as a result, the efficiency of charge transfer decreases.[31] Fig. 5 shows that the spectral characteristics with the increasing thickness narrow and decrease in intensity both in UV and in the visible parts of the spectrum. It can be noted that the effective region of the maximum quantum yield of photocurrent in the visible region is observed at film thicknesses of 150–450 nm. Thus, on thin films of 40–200 nm, as can be seen from the spectra, a greater contribution to the photocurrent is given by visible light, compared to films thicker than 500 nm, where the region of maximum quantum photocurrent yield falls on near UV radiation. In addition, at thicknesses of ~100 nm, the formation of a $SnO_2/BiVO_4$ heterojunction is observed, which is expressed by an increase in the efficiency of the spectral characteristic of the quantum photocurrent yield in the SnO_2 and $BiVO_4$ light absorption regions (Fig. 5). SnO_2 films with a thickness of 250–300 nm have a high electronic conductivity and, having a band gap of 3.1 eV, provide the appearance of photocurrent under UV illumination due to the transmission of light by thin $BiVO_4$ films.

Summarizing the research, we can conclude that for effective light absorption by $BiVO_4$ films it is necessary to grow nanosized crystallites in a matrix of oxides or other vanadates with high electronic conductivity, which will allow you to select the required film thickness for a higher quantum yield of bismuth vanadate fluocurrent and improve the efficiency of such material.

Solid fluoride-conducting electrolytes of composition $Pb_{0.86-x}M_xSn_{1.14}F_{4\pm x}$ (M = Li, Na, K, Rb, Ba, Nd, Sm)

The X-ray diffraction method established that in the system PbF_2–SnF_2 at a ratio of the initial components of 43 mol. % PbF_2 and 57 mol. % SnF_2 forms a single-phase solid solution with the structure β-$PbSnF_4$, the formula of which can be represented as $Pb_{0.86}Sn_{1.14}F_4$.[32] The electrical conductivity of this phase at $T \approx 390$ K is an order of magnitude higher compared to β-$PbSnF_4$ (σ_{373} of 2.9 and 0.902 mS cm^{-1}, respectively). Therefore, in order to search for new substances with improved fluoride-ionic conductivity characteristics, a number of new fluoride-conducting phases based on $Pb_{0.86}Sn_{1.14}F_4$ compound with β-$PbSnF_4$ structure were synthesized by replacing some Pb^{2+} with fluorides of metals of different oxidation states (M = Li, Na, K, Rb, Ba, Nd, Sm).

With partial substitution of Pb^{2+} by M^+, the samples of solid solutions $K_xPb_{0.86-x}Sn_{1.14}F_{4-x}$ (x = 0.03; 0.05; 0.07; 0.10; 0.15) and $Rb_xPb_{0.86-x}Sn_{1.14}F_{4-x}$ were synthesized ($0 < x \leq 0.2$) with crystal lattice of tetragonal syngony of the β-$PbSnF_4$ isostructure (Fig. 6). The substitution of lithium ions leads to the simultaneous formation of two phases: tetragonal (β) and monoclinic (α) modification of $PbSnF_4$. When Pb^{2+} is replaced by Na^+, the reflections are recorded on

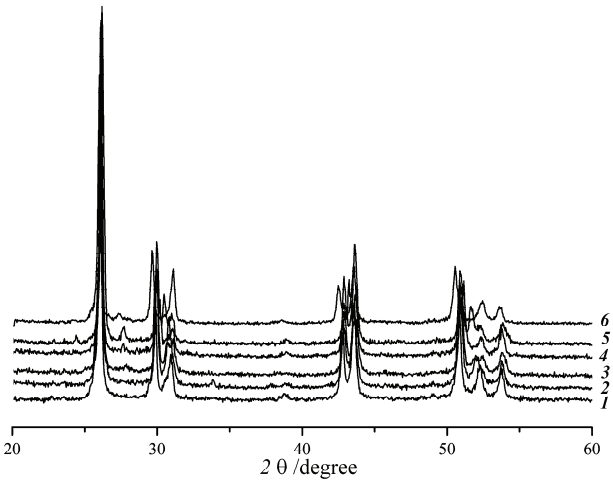

Fig. 6. X-ray diffraction patterns of the synthesized samples: 1 – $Pb_{0.86}Sn_{1.14}F_4$; 2 – $Rb_{0.05}Pb_{0.81}Sn_{1.14}F_{3.95}$; 3 – $K_{0.05}Pb_{0.81}Sn_{1.14}F_{3.95}$; 4 – $Pb_{0.81}Nb_{0.05}Sn_{1.14}F_{4.05}$; 5 – $Pb_{0.76}Sn_{1.14}F_{4.1}$; 6 – $Pb_{0.731}Ba_{0.129}Sn_{1.14}F_4$.

diffractograms even at small amounts of x (up to 3 mol. %), except for the main phase, corresponding to the additional phase of $NaSn_2F_5$, the formation of which, according to literature,[33] leads to a deterioration of the electrical conductivity of the samples.

It was established by the X-ray diffraction method that the partial substitution of Pb^{2+} in the compound $Pb_{0.86}Sn_{1.14}F_4$ by Ba^{2+} forms an uninterrupted series of solid solutions $(Pb_{1-x}Ba_x)_{0.86}Sn_{1.14}F_4$, where x becomes $0 \leq x \leq 1.0$. The symmetry of the crystal lattice of the synthesized phases in the concentration range $0 \leq x \leq 0.50$ corresponds to the structural type β-$PbSnF_4$ (spatial group $P4/nmm$), and with increasing barium fluoride content their crystal lattice is readjusted and approaches the structural type $BaSnF_4$, while preserving the spatial group.

By the X-ray diffraction method, it was found that single-phase solid solutions of the composition $Pb_{0.86-x}R_xSn_{1.14}F_{4+x}$ (R = Nd, Sm) is formed at values of $x \leq 0.15$. When more than 15 mol.% of a rare earth element trifluoride is combined with the structure of the starting compound and the reflexes corresponding to RF_3 are registered on the diffractograms in addition to the main phase, the presence of which in turn can impair the conductive properties of the compounds.

The electrically conductive properties of the synthesized samples of fluoride-conducting phases $M_xPb_{0.86-x}Sn_{1.14}F_{4-x}$ (M = Li, K, Na, Rb) were investigated by the electrochemical impedance spectroscopy. On the impedance diagrams of all studied samples in the high frequency region, only one deformed semicircle is registered, which in the transition to the low-frequency region, and it is transformed into a rectilinear dependence (Fig. 7), which indicates the polarization of the electrolyte/blocking electrode interface.[34] In Fig. 7 the typical impedance hodographs on the example of a solid solution $Rb_xPb_{0.86-x}Sn_{1.14}F_{4-x}$ is shown.

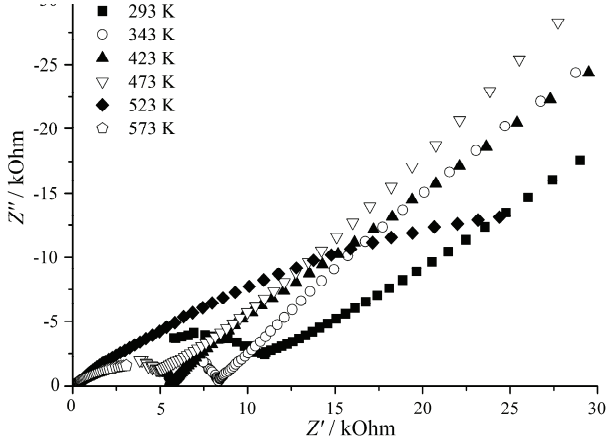

Fig. 7. Impedance diagrams of solid solution $Rb_{0.1}Pb_{0.76}Sn_{1.14}F_{3.9}$ at different temperatures in Nyquist coordinates.

As the temperature increases, the radius of the deformed semicircles decreases (Fig. 7), and the semicircles shift to the region of higher frequencies. At sufficiently high temperatures, the conductivity of the sample can be estimated by analyzing the dependence of the actual component of the complex conductivity on the frequency in Bode coordinates or by the bridge method at frequencies that exclude the influence of blocking electrodes and frequency-dependent impedance component.[34,35] This nature of the change in impedance diagrams is typical for disordered ion-conducting electrolytes with relaxation processes due to the structural and energy inequivalence of charge carriers – fluorides.[36]

The shape of the obtained impedance diagrams indicates the absence of a significant contribution of the conductivity of the crystallite surfaces of the synthesized phases in their total bulk conductivity. This is confirmed by the calculated values of the capacitance of the complex conductivity of the samples at frequencies f_m, which correspond to the maximum values of Z'' of the deformed semicircles. Their value is of the order of 10–40 pF and is much smaller than the conductivity capacity of the crystallite surface 1–100 nF.[36]

Temperature dependencies of fluoride conductivity were studied in the frequency range that is not affected by polarization and relaxation effects. It was found that a slight substitution (up to 3.0 mol. %) of Pb^{2+} on Rb^+ at $T < 500$ K reduces the conductivity of the obtained samples by an order of magnitude, and the nature of its temperature dependence is similar to the temperature dependence of the conductivity of the β-$PbSnF_4$ sample. When replacing 5 mol. % of Pb^{2+} on Rb^+ fluoride-ion the conductivity at $T > 450$ K becomes higher than the conductivity of the initial sample $Pb_{0.86}Sn_{1.14}F_4$, and at temperatures below 450 K – an order of magnitude lower. When lead ions are replaced by rubidium over 0.1 mole fraction, the electrical conductivity in the entire temperature range increases, reaching the maximum values at $x \geq 0.15$. For samples with $x \geq 0.2$, the electrical conductivity practically does not change (Table I). The highest value of conductivity and the lowest activation energy possesses the sample $Rb_{0.3}Pb_{0.56}Sn_{1.14}F_{3.7}$ ($\sigma_{573} = 0.41$ S cm^{-1}, $E_a = 0.16$ eV).

Slight substitution (3.0 mol. %) of Pb^{2+} on K^+ in the structure of $Pb_{0.86}Sn_{1.14}F_4$ causes an increase in electrical conductivity: at 600 K its value is 0.38 S cm^{-1}, and at 330 K – 0.01 S cm^{-1}, which is an order of magnitude higher compared to the original $Pb_{0.86}Sn_{1.14}F_4$ and two orders of magnitude higher compared to pure β-$PbSnF_4$. The activation energy of the electrical conductivity in the high-temperature region does not change (0.08 eV for the original $Pb_{0.86}Sn_{1.14}F_4$ and 0.09 eV for the solid solution $Pb_{0.83}K_{0.03}Sn_{1.14}F_{3.97}$), and the total electrical conductivity increases due to vacancies in the anionic lattice. The electrical conductivity of the synthesized samples with the content of potassium ions, which replace Pb^{2+}, greater than 0.03 mole fraction in the whole temperature range decreases. In contrast to compounds with a purely internodal conduct-

ion mechanism,[34] the activation energy for solid solutions $K_xPb_{0.86-x}Sn_{1.14}F_{4-x}$ at $T > 450$ K increases with the rise of potassium fluoride content. This may be due to the fact that the movement of fluoride ions between vacancies requires more energy than the movement in the interstitial spaces.

TABLE I. Electrical conductivity parameters of the starting compound $Pb_{0.86}Sn_{1.14}F_4$ and solid solutions $Pb_{0.86-x}M_xSn_{1,14}F_{4\pm x}$ (M = Li, Na, K, Rb, Ba, Nd, Sm)

Sample	ΔE_a / eV	σ / S cm^{-1}	T / K
$Pb_{0.86}Sn_{1.14}F_4$	0.28	0.0029	373
	0.18	0.0175	473
	0.1	0.0241	573
$K_{0.03}Pb_{0.83}Sn_{1.14}F_{3.97}$	0.49	0.1200	373
	0.19	0.2870	473
	0.09	0.3730	573
$Rb_{0.2}Pb_{0.66}Sn_{1.14}F_{3.80}$	0.51	0.0772	373
	0.15	0.3400	573
$Pb_{0.43}Ba_{0.43}Sn_{1.14}F_4$	0.11	0.1200	373
	0.11	0.3300	573
$Pb_{0.76}Sm_{0.10}Sn_{1.14}F_{4.10}$	0.36	0.0022	373
	0.26	0.0736	573
$Pb_{0.73}Sm_{0.13}Sn_{1.14}F_{4.13}$	0.31	0.0028	373
	0.43	0.0927	573
$Pb_{0.69}Nd_{0.17}Sn_{1.14}F_{4.17}$	0.1	0.0368	373
	0.34	0.2100	473
	0.18	0.3300	573

The slight substitution ($x = 0.03$) of Pb^{2+} by K^+ in the $Pb_{0.86}Sn_{1.14}F_4$ structure causes an increase in electrical conductivity: at 600 K, its value is 0.38 S cm^{-1} and at 330 K is 0.01 S cm^{-1}, which is an order of magnitude higher compared with original $Pb_{0.86}Sn_{1.14}F_4$ and two orders of magnitude higher compared with pure β-$PbSnF_4$. In this case, the conductivity activation energy in the high-temperature region does not practically change (0.08 eV for original $Pb_{0.86}Sn_{1.14}F_4$ and 0.09 eV for $Pb_{0.83}K_{0.03}Sn_{1.14}F_{3.97}$ solid solution), and the total electrical conductivity increases owing to the appearance of vacancies in the anion sublattice. The electrical conductivity of the synthesized samples with the percentage of potassium ions replacing Pb^{2+} of over $x = 0.03$ decreases over the entire temperature range. Unlike the compounds with purely interstitial conduction mechanism, the activation energy for $K_xPb_{0.86-x}Sn_{1.14}F_{4-x}$ solid solutions at $T > 450$ K increases with potassium and fluoride content.[38] This may be due to the fact that the motion of fluoride ions between vacant positions requires a higher consumption of energy than that in interstitial spaces.

It was found that the substitution of lead ions by Ba^{2+} in the compound $Pb_{0.86}Sn_{1.14}F_4$ at $x \leq 0.30$ leads to a decrease in the electrical conductivity of the obtained samples in comparison with the original compound $Pb_{0.86}Sn_{1.14}F_4$. The

substitution of lead ions at $0.15 \leq x \leq 0.30$ allows a slight increase of the electrical conductivity of the obtained samples only at temperatures above 500 K, compared to the original compound $Pb_{0.86}Sn_{1.14}F_4$. The nature of the temperature dependences of the electrical conductivity is similar to the compound β-$PbSnF_4$.

Subsequent substitution of lead ions in the compound $Pb_{0.86}Sn_{1.14}F_4$ at $x \leq \leq 0.30$ leads to a decrease in the electrical conductivity of the obtained samples in comparison with the original compound $Pb_{0.86}Sn_{1.14}F_4$. Further increase in the content of barium difluoride ($0.30 \leq x \leq 0.55$) increases the electrical conductivity of the synthesized samples in the entire temperature range. The sample with the highest electrical conductivity and the lowest activation energy of ionic conductivity is $Pb_{0.43}Ba_{0.43}Sn_{1.14}F_4$ (σ = 0.12 S cm^{-1}, E_a = 0.11 eV at 373 K). In this case, the replacement of half of the lead ions by barium ions in the compound $Pb_{0.86}Sn_{1.14}F_4$ allows the electrical conductivity to increase more than 100 times compared to the conductivity of the initial phase of β-$PbSnF_4$.

The introduction to 8 mol. % SmF_3 in the initial structure $Pb_{0.86}Sn_{1.14}F_4$ helps to reduce the electrical conductivity of the obtained samples in the entire temperature range compared to $Pb_{0.86}Sn_{1.14}F_4$, bringing them closer to the values of electrical conductivity of β-$PbSnF_4$. However, at temperatures above 520 K the electrical conductivity of solid solutions is almost three times higher than the value for β-$PbSnF_4$ (σ_{553} = 0.054 and 0.017 S cm^{-1}, respectively) and twice higher than the electrical conductivity of the original compound $Pb_{0.86}Sn_{1.14}F_4$ (σ_{553} of 0.054 and 0.023 S cm^{-1}, respectively). A further increase in the concentration of Sm^{3+} in the structure of the initial fluoride $Pb_{0.86}Sn_{1.14}F_4$ leads to an increase in electrical conductivity in the entire temperature range. The most significant effect of the heterovalent substituent is manifested at temperatures above 420 K. For example, the value of electrical conductivity for solid solutions $Pb_{0.76}Sm_{0.10}Sn_{1.14}F_{4.10}$ and $Pb_{0.73}Sm_{0.13}Sn_{1.14}F_{4.13}$ at T = 500 K is 0.038 and 0.046 S cm^{-1}, respectively, while for the compound $Pb_{0.86}Sn_{1.14}F_4$ it is 0.02 S cm^{-1}.

Slight substitution (3.0 mol. %) of Pb^{2+} by Nd^{3+} in the structure of $Pb_{0.86}Sn_{1.14}F_4$ causes an increase in electrical conductivity at $T > 530$ K (68.8 mS cm^{-1} compared with 24.1 mS cm^{-1} for the initial compounds $Pb_{0.86}Sn_{1.14}F_4$), and below this temperature, on the contrary, slightly reduces the electrical conductivity, approaching the values of β-$PbSnF_4$. The activation energy of the conductivity increases in the whole temperature range. With a further increase in the content of Nd^{3+} the fluoride-ion conductivity of the samples increases throughout the temperature range. It should be noted that samples with a content of 10–15 mol. % NdF_3 at $T > 500$ K have comparable values of electrical conductivity, and below this temperature, it increases with the substituent content. The compound $Pb_{0.69}Nd_{0.17}Sn_{1.14}F_{4.17}$ has the highest values of electrical conductivity and the lowest activation energy. The subsequent introduction of neodymium trifluoride (more than 18 mol. %) into the $Pb_{0.86}Sn_{1.14}F_4$ structure leads

to a decrease in the electrical conductivity of the samples, which can be explained by the formation of an additional NdF_3 phase, as evidenced by the results of X-ray phase analysis.

Thus, it is found that the substitution in the composition of the fluoride-conducting phase $Pb_{0.86}Sn_{1.14}F_4$ part of the cations of lead (up to 20 mol.%) increases its conductivity in the entire temperature range, and to a greater extent, the higher the concentration of the substituent. The highest conductivity and the lowest activation energy have samples of the composition $Pb_{0.69}Nd_{0.17}Sn_{1.14}F_{4.17}$ (σ_{373} = 0.0368 S cm^{-1}), $Pb_{0.76}Sm_{0.10}Sn_{1.14}F_{4.10}$ and $Pb_{0.73}Sm_{0.13}Sn_{1.14}F_{4.13}$ (σ_{500} of 0.038 and 0.046 S cm^{-1}, respectively), $K_{0.03}Pb_{0.83}Sn_{1.14}F_{3.97}$ (σ_{600} = 0.38 S cm^{-1}, σ_{330} = 0.01 S cm^{-1}), $Rb_{0.2}Pb_{0.63}Sn_{1.14}F_{3.8}$ σ_{573} in range 0.34–0.41 S cm^{-1}, E_a = 0.16 eV and σ_{373} in range 53.4–81.6 mS cm^{-1}, E_a = 0.48 to 0.51 eV in accordance). The transfer numbers for fluorine anions are not less than 0.99 and practically do not depend on the concentration of the substituent.

Lithium iron phosphate as a promising cathode material

Recently, much attention has been paid to systems based on low-temperature deep eutectic solvents (DES), which differ from other ionic liquids. In recent years, DES has begun to be considered as a design solvent for the development of nanomaterials with a well-defined morphology, including nanoparticles with a controlled structure.

It should be noted that of particular interest for the synthesis of cathode materials is the DES composition: choline chloride–ethylene glycol (ChCl–EG), choline chloride–diethylene glycol (ChCl–DEG), choline chloride–triethylene glycol (ChCl–TEG). This system has all the advantages of solvothermal synthesis in ethylene glycol, diethylene glycol, triethylene glycol, which are characterized by high boiling points 473–573 K, the ability to dissolve polar inorganic salts, to form chelated complexes with transition metals. They also provide a reducing reaction medium. Due to these unique physicochemical properties, these glycols can affect the kinetics of the chemical reaction and the morphology of the precipitates obtained in the synthesis of nanomaterials. They are not only solvents and reducing agents, but also play the role of a template for directional growth and self-assembly of hierarchical structures in the formation of nanocrystals. At the same time, DES is characterized by a number of special properties that distinguish them from other ionic liquids and polyols: they are cheap and readily available, non-toxic, and extremely easy to prepare. In addition, DES based on ChCl and the above-mentioned polyhydric alcohols readily dissolve oxides and salts of many metals that are insoluble or sparingly soluble in other ionic liquids.

To obtain such compounds, in particular $LiFePO_4$, the method of synthesis by ion exchange reaction was used by using $NH_4FePO_4 \cdot H_2O$ as a base precursor. The similarity of the crystal structure of $NH_4FePO_4 \cdot H_2O$ and $LiFePO_4$ allows

the synthesis of $LiFePO_4$ by replacing the NH_4^+ in NH_4FePO_4 with the Li^+ from the lithium salt.

Synthesis of $LiFePO_4$ with thermal heating in choline chloride and DEG was performed on a magnetic stirrer with a thermostat and the ability to heat up to 623 K. A mixture of choline chloride and ethylene glycol or choline chloride and triethylene glycol (1:2) was placed in a heat resistant Simax conical flask under reflux condenser and kept for 1 h at 353 K and 300 rpm. Then ammonium iron (II) phosphate was added, and the lithium precursor was heated to 473–573 K and kept for 1 to 4 h. Upon completion of the synthesis, the precipitate was washed in distilled water and isopropyl alcohol. The resulting powder was dried for 2 h at a temperature of 393 K. The precipitation of $LiFePO_4$ occurs with the formation and evaporation of gaseous reaction products: NH_3, CH_3COOH and H_2O. The ion exchange reaction occurs by replacing the NH_4^+ in $NH_4FePO_4 \cdot H_2O$ with a Li^+ from lithium acetate. Compared with the usual solid-phase reaction, the ion exchange reaction in EG–choline chloride/TEG–choline chloride does not require high temperatures and occurs in a short time.

At a temperature of 473 K in choline chloride–ethylene glycol and a synthesis time of 1 to 4 h, the precipitates obtained are amorphous in nature with a low content of crystalline phase, as evidenced by radiographs with a characteristic halo for amorphous samples (Fig. 8b). The powder synthesized in the environment of choline chloride–triethylene glycol at a temperature of 573 K is characterized by sufficient crystallinity after the first hour of synthesis (Fig. 8a). In the obtained samples there are no impurities (within the sensitivity of the method), all reflexes are consistent with the standard JCPDSNo: 00-40-1499. The excess of precursor lithium in the reaction medium does not affect the composition of the final product.

To synthesize the composite cathode material with carbon, $LiFePO_4$ powders were wetted with glucose solution, dried at 323 K, and placed in a quartz reactor, where it was annealed at 973 K. under argon for 1 h. The carbon content in the composite was determined using gravimetric methods. To find out the theoretical content of carbon formed after the carbonization of glucose or malic acid during the production of the composite, the samples of organic components

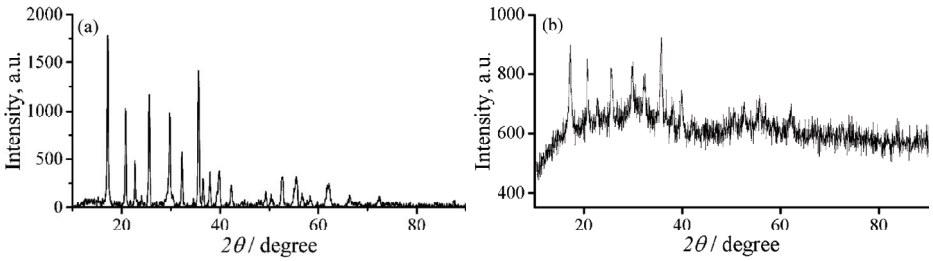

Fig. 8. XRD spectra of $LiFePO_4$ synthesized in ChCl-TEG (A) ChCl-EG (B).

were subjected to heat under conditions corresponding to the annealing regime of $LiFePO_4$. Based on the obtained results, the masses of glucose or malic acid were calculated, which were added to the synthesized powder for further annealing and obtaining a composite. With the introduction of the organic component with the calculation of the formation of 10 wt. % C after annealing, in practice the results range from 9.8 to 10.1 %, which is due to losses and inaccuracies of measurement during the experiment.

X-ray photoelectron spectroscopy (XPS) was used to study the surface of the synthesized cathode material – $LiFePO_4$ and carbon composite based on it – $LiFePO_4$/C. A study of Fe $2p_{3/2}$ spectra of $LiFePO_4$ and $LiFePO_4$/C composite obtained at 973 K for 1 h was performed.[38] The spectra of Fe $2p_{3/2}$ levels are formed by components in the region 709.6–711.3 eV, which belong to Fe^{2+} states of Fe, and components in the region 712.6 to 714.5 eV to Fe^{3+} states in $LiFePO_4$.

Galvanostatic charge/discharge characteristics of the electrode based on $LiFePO_4$ were taken using a 1 M electrolyte based on $LiPF_6$ in EC:DMC (1:1) in a cell type "coin cell". Fig. 9a shows the second and third cycles of charge/discharge. The material capacity for the second cycle is about 130 mAh g^{-1}, and for the 3rd ~120 mAh g^{-1}. Continuation of the cycle did not occur due to violation of the integrity of the cell and the probable decomposition of the electrolyte and the formation of dendrites.

For the material $LiFePO_4$/C with a carbon content of ~10 %, the charge/discharge characteristics were obtained in a T-shaped cell with an electrolyte composition: 0.6 M solution of bis (oxalate) lithium borate (LiBOB) in an equimolar mixture of EC–DMC. The capacity of the material in terms of the content of pure $LiFePO_4$ in the cathode mass is about 100 mAh g^{-1} for the best cycle at a current of 0.1*C* (Fig. 9b). It was not possible to carry out a large number of cycles, which is explained by imperfect assembly conditions and insufficiently clean materials, first of all by the quality of the electrolyte and the "wear" of the cell, which does not ensure tightness. Also, long-term annealing of the material leads to a slight

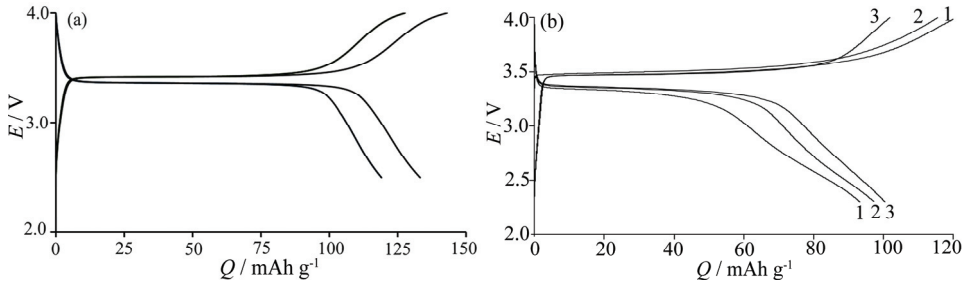

Fig. 9. Charge/discharge characteristics of the electrode based on $LiFePO_4$/C; a) in a 1 M solution of $LiPF_6$ in EC: DMC (1:1) at a current of 0.1*C*; b) in a 0.6 M solution of LiBOB in EC: DMC (1:1) at a current of 0.1*C* for three cycles.

oxidation of the powder surface, which could lead to the formation of unwanted impurities and slightly underestimate the electrochemical parameters of the material in terms of the content of $LiFePO_4$ in the cathode mass.

It should be noted that the functional characteristics of $LiFePO_4$ depend significantly on the materials and assembly methods of the electrochemical cell. Unfortunately, our material and technical conditions for testing electrode materials are imperfect. Therefore, we obtain underestimated results, which is confirmed by the results of testing commercial $LiFePO_4$ under our assembly conditions.[37] For commercial material ($LiFePO_4$/C "Life Power P1" Phostech Lithium inc., Canada) the capacity is 140 mAh g^{-1}, but under the conditions we worked in, it was 120 mAh g^{-1} when using a coin cell.[37] For comparison, the best material synthesized by us had capacity indicators of ~130 mAh g^{-1}.

CONCLUSION

Monoclinic $BiVO_4$ films were obtained by electrochemical synthesis. The composition of the film material was determined by X-ray diffraction and EDAX. It has been established that for the efficient absorption of light by $BiVO_4$ films, it is necessary to grow nanosized crystallites in a matrix of oxides or other vanadates with high electronic conductivity. A study of the effect of the thickness of $BiVO_4$ films obtained by electrochemical deposition on the quantum yield of photocurrent showed that for the most effective increase in photocurrent from 0.25 such photo anodes, thin $BiVO_4$ films of 150-400 nm should be used.

It was confirmed that the substitution of part of lead cations (up to 20 mol. %) in the composition of the fluoride-conducting phase $Pb_{0.86}Sn_{1.14}F_4$ helps to increase its conductivity in the entire temperature range, and the greater the concentration of the substitute, to a greater extent. The transfer numbers for fluorine anions are not lower than 0.99 and practically do not depend on the concentration of the substituent.

Composite materials with carbon based on lithium ferrum (II) phosphate ($LiFePO_4$/C) were obtained in the environment of DES (low-temperature eutectic solvents): choline chloride-triethylene glycol (ChCl–TEG) and choline chloride––ethylene glycol (ChCl–EG), using NH_4FePO_4 and CH_3COOLi as precursors. Electrochemical studies of the obtained materials were carried out using a t-cell of our own production and a "coin cell" type cell with electrolytes based on commercial $LiPF_6$ and self-synthesized LiBOV. The best results (capacity based on pure $LiFePO_4$ is ~130 mAh g^{-1} for a current of 0.1*C*) were obtained for powders synthesized in ChCl–TEG and annealed for 1 h at 973 K with a carbon content of ~10 %. Powder ($LiFePO_4$/C) with a carbon content of ~10 % synthesized in an environment of ethylene glycol and choline chloride with subsequent annealing for 10–12 h at 973 K in an argon atmosphere showed worse results: in terms of $LiFePO_4$, the capacity was ~100 mAh g^{-1} for a current of 0.1*C*.

ИЗВОД

ВИСОКО ЕФИКАСНИ ФУНКЦИОНАЛНИ МАТЕРИЈАЛИ ЗА САВРЕМЕНЕ ЕЛЕКТРОХЕМИЈСКЕ УРЕЂАЈЕ

VITALY SMILYK, YULIIA VOLOSHANOVSKA, VADYM GALAGUZ, OLEKSANDR IVANENKO и OLHA MEDVEZHYNSKA

V. I. Vernadsky Institute of General and Inorganic Chemistry of the National Academy of Sciences of Ukraine, 32-34 Acad. Palladina Ave., Kyiv, 03142, Ukraine

У потрази за новим функционалним материјалима и материјалима побољшаних перформанси за електрохемијске уређаје нове генерације, синтетисано је неколико нових материјала. Конкретно, филмови $BiVO_4$ су добијени електрохемијском синтезом, при чему је коришћена интерферометријска контрола дебљине филма током таложења. Претходно је нађено да је најефикасније коришћење танких филмова $BiVO_4$ дебљине 150–400 nm, код којих је запажен пораст квантног приноса фотострује до 0,25 на таласној дужини 400–450 nm. $LiFePO_4$ је синтетисан из нискотемпературне еутектичке смеше холин-хлорид–триетилен-гликол (ChCl–TEG) и холин-хлорид–етилен-гликол (ChCl–EG) коришћењем NH_4FePO_4 and CH_3COOLi као прекурсора. Показано је да примењени режим синтезе $LiFePO_4$/C на 973 K током 1 h не доводи до оксидације $LiFePO_4$, јер је однос Fe^{2+}/Fe^{3+} у $LiFePO_4$ и у $LiFePO_4$/C био 2,4 и 2,7, редом. Утврђено је да замена дела катјона олова (до 20 mol. %) у проводној фази $Pb_{0,86}Sn_{1,14}F_4$ доприноси повећању његове проводљивости у целом температурном опсегу, и у већој мери повећаној концентрацији супституента. Пренос наелектрисања је обезбеђен високо покретљивим интерситицијалним флуоридним анјонима, чија концентрација расте са повећањем темературе и садржаја супституента.

(Примљено 27. јула, ревидирано 15. новембра, прихваћено 20. новембра 2022)

REFERENCES

1. N. Nitta, F. Wu, *Mater. Today* **18** (2015) 252 (https://doi.org/10.1016/j.mattod.2014.10.040)
2. T. L. Kulova, *Russ. J. Electrochem.* **49** (2013) 25 (https://doi.org/10.1134/S1023193513010102)
3. X. Kang1, *Chem. Rev.* **104** (2004) 4303 (https://doi.org/10.1021/cr030203g)
4. M. S. Whittingham, *Chem. Rev.* **104** (2004) 4271 (https://doi.org/10.1021/cr020731c)
5. A. B. Yaroslavtsev, T. L. Kulova, *Uspekhi khimii* **84** (2015) 826 (https://doi.org/10.1070/RCR4497)
6. X. Li, B. Yue, *App. Catal., A* **390** (2010) 2195 (https://doi.org/10.1016/j.apcata.2010.10.013)
7. G. Teran-Escobar, J. Pampel, *Energy Environ. Sci.* **6** (2013) 3088 (https://doi.org/10.1039/C3EE42204F)
8. Z. Yang, Y. Li, *J. Catal.* **280** (2011) 247 (https://doi.org/10.1016/j.jcat.2011.03.026)
9. H. Miyake, H. Kozuka, *J. Phys. Chem., B* **109** (2005) 17951 (https://doi.org/10.1021/jp058051b)
10. N. I. Sorokin, B. P. Sobolev, *Kristallografiya* **52** (2007) 870 (https://naukarus.com/nestehiometricheskie-ftoridy-tverdye-elektrolity-dlya-elektrohimicheskih-ustroystv-obzor)
11. L. N. Patro, K. Hariharan, *Solid State Ionics* **239** (2013) 41 (https://doi.org/10.1016/j.ssi.2013.03.009)

12. V. Trnovtsova, P. P. Fedorov, *Elektrokhimiya* **45** (2009) 668 (https://naukarus.com/ftoridnye-tverdye-elektrolity)
13. J. Resasco, H. Zhang, *ACS Cent. Sci.* **2** (2016) 80 (https://doi.org/10.1021/acscentsci.5b00402)
14. J. Gan, X. Lu, *Nanoscale* **16** (2014) 7142 (https://doi.org/10.1039/C4NR01181C)
15. V. O. Smilyk, S. S. Fomanyuk, G. Ya. Kolbasov, I. A. Rusetskyi, V. S. Vorobets, *Res. Chem. Intermed.* **45** (2019) 4149 (https://doi.org/10.1007/s11164-019-03897-y)
16. Y. Li, J. Zhu, *Sci. Chin. Chem*. **9** (2014) 1489 (https://doi.org/10.1007/s11426-015-5348-3)
17. Z. Yang, Y. Dai, *J. Mater. Chem., A* **4** (2016) 8210 (https://doi.org/10.1039/C6TA05048D)
18. L. X. Yuan, Z. H. Wang, *Energy Environ. Sci.* **4** (2011) 269 (https://doi.org/10.1039/C0EE00029A)
19. U. S. Kasavajjula, C. Wang, *J. Electrochem. Soc.* **155** (2008) A866 (https://doi.org/10.1149/1.2980420)
20. T. V. Satyavani, A. K. Srinivas, *Eng. Sci. Tech.* **19** (2016) 178 (https://doi.org/10.1016/j.jestch.2015.06.002)
21. T. Kodera, B. Dongying, *Key Eng. Mater.* **485** (2011) 107 (https://doi.org/10.4028/www.scientific.net/KEM.485.107)
22. Y. Lin, M. X. Gao, *J. Power Sources* **184** (2008) 444 (https://doi.org/10.1016/j.jpowsour.2008.03.026)
23. V. O. Smilyk, S. S. Fomanyuk, *Ukrayins'kyy khimichnyy zhurnal* **85** (2019) 83 (https://doi.org/10.33609/0041-6045.85.10.2019.83–90)
24. Ye.V. Kuzminskii, G.Ya. Kolbasov, *Sol. Energ. Mater. Sol. Cells* **56** (1999) 93 (https://doi.org/10.1016/S0927-0248(98)00146-9)
25. T. Saison, N. Chemin, *J. Phys. Chem.* **119** (2015) 12967 (https://doi.org/10.1021/acs.jpcc.5b01468)
26. R. Katoh, M. Kasuya, *Chem. Phys. Lett.* **471** (2009) 280 (https://doi.org/10.1016/j.cplett.2009.02.053)
27. C. A. Grimes, G. K. Mor, *TiO_2 Nanotube Arrays. Synthesis, Properties, and Applications,* Springer, New York, 2009, p. 358 (https://doi.org/10.1007/978-1-4419-0068-5)
28. R. Sharma, P.P. Das, *Nanotechnology* **20** (2009) 075704 (https://doi.org/10.1088/0957-4484/20/7/075704)
29. C. G. Granqvist, *Handbook of Inorganic Electrochromic Materials,* Elsevier, Uppsala, 1995 (https://doi.org/10.1016/B978-0-444-89930-9.X5000-4)
30. N. N. Dinh, D. H. Ninh, *J. Nanomat*. **2012** (2012) 7 (https://doi.org/10.1155/2012/781236)
31. M. F. Saenger, T. Höing, *Phys. Status Solidi, A* **4** (2008) 914 (https://doi.org/10.1002/pssa.200777894)
32. Yu. V. Pohorenko, R. M. Pshenychnyi, *J. Serb. Chem. Soc.* **86** (2021) 845 (https://doi.org/10.2298/JSC201124031P)
33. S. S. Fomanyuk, V. O. Smilyk, *Fr.-Ukr. J. Chem.***06** (2018) 157 (https://doi.org/10.17721/fujcV6I1P157-166)
34. Q. Jia, K. Iwashina, *Proc. Natl. Acad. Sci. USA* **109** (2012) 11564 (https://doi.org/10.1073/pnas.1204623109)
35. D. K. Lee, K.-S. Choi, *Nat. Energy* **3** (2018) 53 (https://doi.org/10.1038/s41560-017-0057-0)

36. M. G. Mali, H. Yoon, *Appl. Phys. Lett.* **106** (2015) 151603 (https://doi.org/10.1063/1.4918583)
37. O. Bohnke, C. Bohnke, *Solid State Ionics* **6** (1982) 267 (https://doi.org/10.1016/0167-2738(82)90048-0)
38. V. Galaguz, O. Korduban, *J. Serb. Chem. Soc.* **85** (2020) 1047 (https://doi.org/10.2298/JSC190910011G).